Thin-Film Metastable Oxides

DOI: 10.1002/anie.200700119

Unit-Cell-Level Assembly of Metastable Transition-Metal Oxides by Pulsed-Laser Deposition**

*Lei Yan, Hongjun Niu, Craig A. Bridges, Paul A. Marshall, Joke Hadermann, Gustaav van Tendeloo, Paul R. Chalker, and Matthew J. Rosseinsky**

Classical solid-state synthesis methods allow access to many complex extended structures, which can be classified in terms of basic structural units.[1] This understanding can then be used to identify further compositions and structures for synthesis. For example, a modular structural approach can be used to guide the synthesis of superconducting copper oxides.[2] One limitation is the availability of synthetic methods that will permit the *isolation* of the identified structures. Conventional solid-state synthesis involving a diffusional reaction between powders ground to dimensions of the order of microns often requires elevated temperatures to permit diffusion of the reacting atoms at a sufficient rate to form the desired structure. With the exception of generalized kinetically controlled routes, such as intercalation into a pre-existing host,[3] this approach usually leads to the formation of thermodynamically controlled products. In this case, the absence of a direct structural relationship between the reagents and products hinders targeted synthesis. This situation has led to the development of kinetically controlled approaches to materials assembly,[4] involving the pre-assembly of disordered reagents to direct low-temperature crystallization,[5,6] or the atom-by-atom construction of materials by molecular-beam epitaxy (MBE),[7] for example. MBE and the related process pulsed-laser deposition (PLD) are frequently associated with the deposition of epitaxial semiconductor device structures, but they can also be exploited to prepare new multilayered materials (e.g., ABO_3 perovskites with controlled B-site cation order[8–10]), opening up exciting prospects for synthetic solid-state chemistry. Herein, we report the targeted synthesis of the $n=4$, 5, and 6 members of the $Ca_{n+1}Mn_nO_{3n+1}$ Ruddlesden–Popper (RP) series by the assembly of the constituent modules ($CaMnO_3$ perovskite and CaO rock-salt blocks) in a unit-cell-upon-unit-cell manner, with in situ monitoring of the growth process using reflection high-energy electron diffraction (RHEED).[11]

The RP series $A_{n+1}B_nO_{3n+1}$ (or $AO(ABO_3)_n$) is one of the simplest lending itself to the modular-assembly approach. There are two structural components: an AO rock-salt layer, which is electrically insulating, and an ABO_3 perovskite layer n-octahedra thick (Figure 1). In principle, the value of n is indefinitely variable, but ceramic routes to oxides typically only afford $n=3$ as the maximum finite value. The relatively

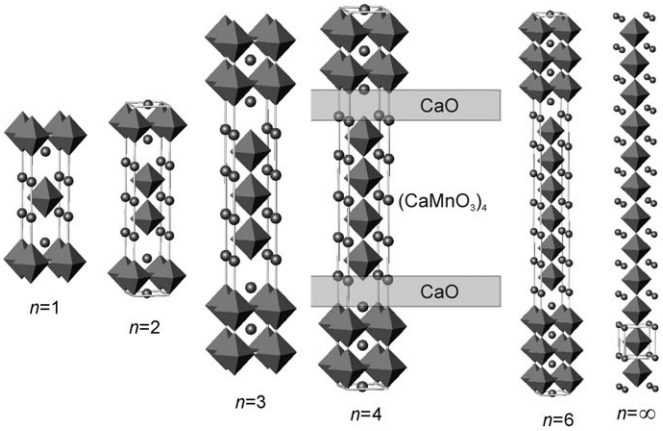

Figure 1. The Ruddlesden–Popper (RP) series $A_{n+1}B_nO_{3n+1}$ can be viewed as an assembly of AO rock-salt and ABO_3 perovskite layers. The unit cells of the $n=1$–6 and ∞ members of the $Ca_{n+1}Mn_nO_{3n+1}$ (or $CaO(CaMnO_3)_n$) RP family are shown. The MnO_6 octahedra are shown as polyhedra and the Ca^{2+} ions as spheres.

small mismatch between the Sr–O distances in SrO itself and in $SrTiO_3$ has permitted the growth of the $n=4$ and $n=5$ members of $Sr_{n+1}Ti_nO_{3n+1}$ on $SrTiO_3$ substrates by MBE[12] and by RHEED-assisted PLD.[13] There has been little progress in growing thin films of other RP structures, except the deposition of both c-axis[14–16]- and (110)[17]-oriented $(La,Sr)_3Mn_2O_7$ ($n=2$) thin films. An $n=4$ RP phase in the $Sr_{n+1}Co_nO_{3n+1}$ series has been prepared under high pressure.[18]

The inaccessibility of higher-n members in the manganate RP family is a particularly serious limitation, as higher n values offer a route to increased magnetic-ordering temperatures in these "natural spin-valve" structures of interest for tunneling magnetoresistance.[19] As PLD is a versatile route to intergrowing unit cells with different metal compositions,[9,20] it permits, in principle, the modular assembly of different

[*] Dr. L. Yan, Dr. H. Niu, Dr. C. A. Bridges, Prof. M. J. Rosseinsky
Department of Chemistry
University of Liverpool, Liverpool L69 7ZD (UK)
Fax: (+44) 151-794-3587
E-mail: m.j.rosseinsky@liv.ac.uk
Dr. P. A. Marshall, Prof. P. R. Chalker
Department of Engineering
University of Liverpool, Liverpool L69 3GH (UK)
Prof. J. Hadermann, Prof. G. van Tendeloo
Electron Microscopy for Materials Science
University of Antwerp
Groenenborgerlaan 171, 2020 Antwerp (Belgium)

[**] We thank the EPSRC for funding under EPSRC/C511794 and Dr. S. Lee (Department of Physics, University of Liverpool) for assistance with the X-ray characterization of the films.

Supporting information (Experimental Section and supplementary Figures) for this article is available on the WWW under http://www.angewandte.org or from the author.

structural units in direct relationship to the way a synthetic solid-state chemist would propose the structure and composition of a new material.

The $n=4$ RP manganate $Ca_5Mn_4O_{13}$ is inaccessible in the bulk, as classical high-temperature synthesis affords phase separation into $Ca_4Mn_3O_{10}$ ($n=3$) and $CaMnO_3$ ($n=\infty$). Epitaxial strain imposed by the substrate is important in stabilizing, in thin-film form, materials that are otherwise metastable under classical synthesis conditions.[21] This work uses $SrTiO_3(100)$ substrates pretreated through the homoepitaxial growth of 22 layers of $SrTiO_3$ (600 laser pulses) to give a 2×1 reconstructed surface (Figure S1 in the Supporting Information).[22] The $SrTiO_3$ (STO; $a_{STO}=3.905$ Å) substrate has a lattice mismatch of 4.5% with $CaMnO_3$ ($a_{CaMnO_3}=3.730$ Å), while the Ca–O bond length in the rock-salt structure CaO ($a_{CaO}=4.815$ Å) has a mismatch of 12.8% with the Sr–O distance in the perovskite $SrTiO_3$. The strain-stabilization approach is unsuccessful here in stabilizing $Ca_5Mn_4O_{13}$. PLD growth on the $SrTiO_3(100)$ substrate from a single-source biphasic bulk target with the $Ca_5Mn_4O_{13}$ ($n=4$) composition affords instead an epitaxial *c*-axis-oriented film with the perovskite ($n=\infty$) structure. We therefore adopted the alternative approach of layer-by-layer assembly of the $n=4$ RP structure from pseudomorphically strained individual unit cells of $CaMnO_3$ and CaO deposited from two separate targets.

The reconstructed $SrTiO_3(100)$ surface is suitable for the growth of the $n=4$ RP manganate, if precise control of the layer-by-layer growth is maintained to take into account the differences in bond length at the interfaces formed during the growth process. The strain introduced by the deposition of CaO onto the $SrTiO_3$ substrate leads to the disappearance of the RHEED pattern after 150 laser pulses, owing to relaxation of the coherent film structure driven by the large bond-length mismatch referred to above. However, the mismatch between the A–O distance in the cubic CaO structure (2.408 Å) and that in the $CaMnO_3$ perovskite (2.637 Å) is significantly less (−8.7%) than the bond-length mismatch between CaO and $SrTiO_3$. Similarly, the small difference in cell parameters between $CaMnO_3$ and $SrTiO_3$ permits epitaxial growth. By starting the growth of the target $n=4$ RP structure with the deposition of four unit cells of $CaMnO_3$ on the $SrTiO_3(100)$ substrate at 800 °C, it is possible to introduce a buffer $CaMnO_3$ layer before the first CaO layer to decrease the mismatch. The success of the subsequent deposition then depends on whether precisely one CaO layer can be deposited on top of this first module of the target $n=4$ structure. Either insufficient or excessive deposition of CaO compared with the quantity required to form a single-unit-cell layer (or unit) prevents the subsequent formation of the whole superlattice, leading instead to a thin film with the perovskite structure (Figure S2). In particular, termination of the deposition of the CaO layer before precisely one single-unit-cell layer is stabilized affords either epitaxial perovskite films or systems with extremely broad low-angle diffraction features consistent with the formation of very small domains of the target RP structure. The deposition of the first CaO layer and subsequent CaO and $(CaMnO_3)_n$ units requires the reduction of the substrate temperature to 700 °C to maintain the RHEED oscillations indicating layer-by-layer growth. Figures 2 and S3 show RHEED oscillations during the growth of the $Ca_{n+1}Mn_nO_{3n+1}$ ($n=4$, 5, and 6) materials deposited according to the ideal sequence with complete CaO-layer coverage at a 700 °C growth temperature in 2.8×10^{-4} Torr O_2.

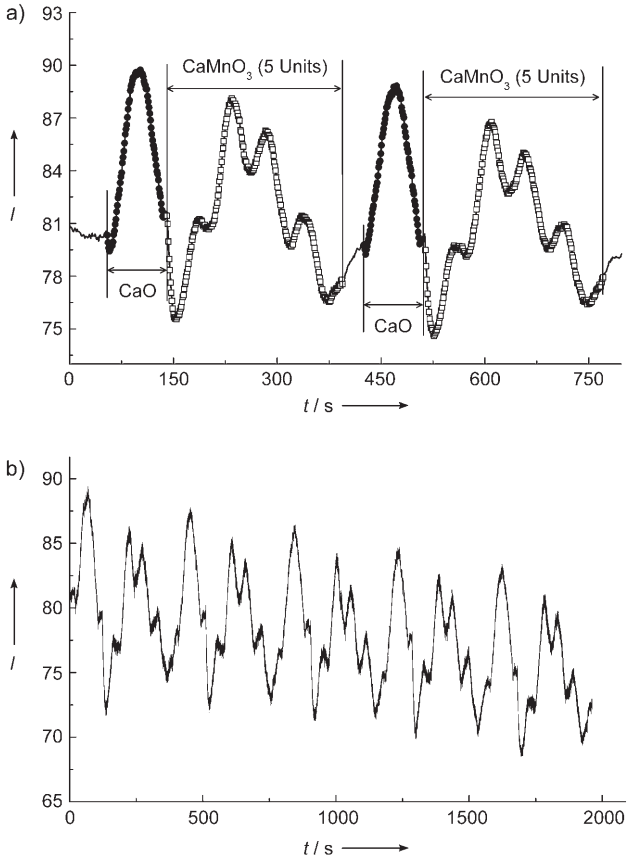

Figure 2. RHEED oscillations measured for a) 2 periods and b) 5 periods of the PLD deposition of the CaO and $(CaMnO_3)_5$ layers during the growth of the $Ca_6Mn_5O_{16}$ phase ($n=5$). The filled and empty symbols in (a) indicate the CaO and $CaMnO_3$ deposition periods, respectively. The persistence of the RHEED oscillations without significant damping indicates that the superlattice has been grown epitaxially.

From these RHEED oscillations, one can clearly follow the deposition process at the unit-cell scale as illustrated for $n=5$ $Ca_6Mn_5O_{16}$ in Figure 2. As the CaO layer is deposited, the RHEED intensity increases initially with an increasing number of laser pulses. Finally, it reaches its maximum value, and then decreases. The point at which the RHEED intensity decreases to the same level as its original value corresponds to the deposition of one complete single-unit-cell CaO layer. At this stage, the laser is switched to the $CaMnO_3$ target and the RHEED intensity decreases as the first $CaMnO_3$ layer grows. The subsequent increase to a maximum value corresponds to the deposition of one complete single-unit-cell $CaMnO_3$ layer. There are five clear periods in the RHEED oscillations during $CaMnO_3$ deposition in the case of the $n=5$ film (Figure 2a), which indicates that five single-unit-cell $CaMnO_3$ layers have been grown. The initial growth of five $CaMnO_3$

units is essential to permit the subsequent growth of the epitaxial RP phase with smooth interfaces between the coherent layers. The initial deposition of four and six $CaMnO_3$ units, respectively, permits the growth of the $n=4$ and $n=6$ members of the RP series (Figures 1 and S3)

We can clearly distinguish that all the films are in the *c*-axis orientation and have the desired RP structure for each member of the series. The XRD patterns of the $Ca_{n+1}Mn_nO_{3n+1}$ films with $n=4$, 5, and 6 are shown in Figure 3. Small quantities of perovskite intergrowth are

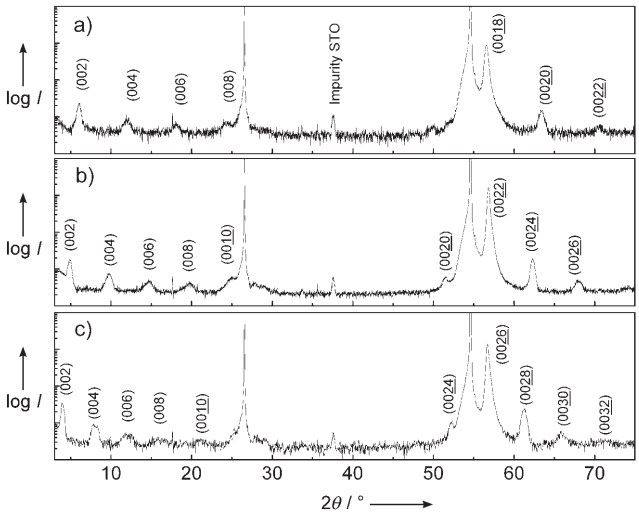

Figure 3. X-ray diffraction patterns of thin films of the RP phases $Ca_{n+1}Mn_nO_{3n+1}$ with a) $n=4$, b) $n=5$, and c) $n=6$. The intense unindexed reflections are from the $SrTiO_3$ (100) (STO) substrate.

visible (Figure S4a). The rocking curve for the (0018) reflection of the $n=4$ film (Figure S4b) further demonstrates that a high degree of *c*-axis epitaxial orientation has been achieved. The *c*-axis lattice parameter is (34.12 ± 0.02), (41.46 ± 0.04), and (49.11 ± 0.07) Å for the $n=4$, 5, and 6 RP phases, respectively. As these compounds are not known as bulk phases, it is necessary to compare them with the trend in the lattice parameters of 12.05, 19.575, and 27.119 Å reported for the bulk $n=1$, 2, and 3 RP phases. Values of approximately 34.65, 42.19, and 49.72 Å would be expected for the $n=4$, 5, and 6 phases in the absence of strain or of variations in composition and octahedral tilting.[23] In the present thin-film case, the in-plane tensile stress on the RP lattice due to the larger a_{STO} lattice parameter will cause an out-of-plane compression, contributing to a slight decrease in the *c*-axis lattice parameter compared with the expected values.

The high-resolution transmission electron microscopy (HRTEM) image in Figure 4a confirms the growth of the $Ca_5Mn_4O_{13}$ ($n=4$) layers shown by XRD. Under the given defocus conditions, the dark dots in the image correspond to projected cation columns in the structure. Image simulations confirm that the brighter (horizontal) rows correspond to the rock-salt CaO layers.

At the $SrTiO_3$–$Ca_5Mn_4O_{13}$ interface, lattice misfit occurs owing to the rock-salt bond-length mismatch; this misfit is

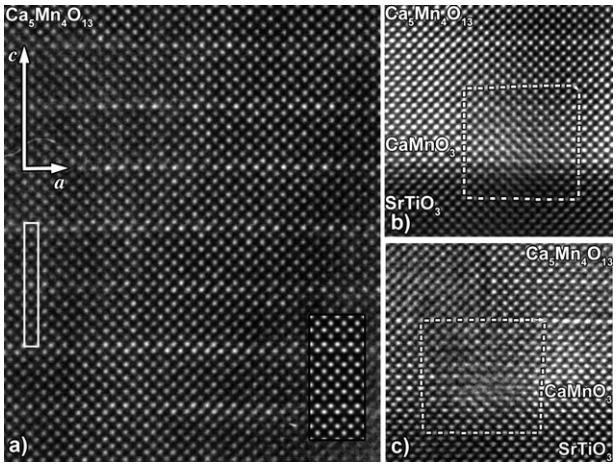

Figure 4. Cross-sectional HRTEM images of the epitaxially grown RP phase $Ca_5Mn_4O_{13}$ ($n=4$). a) Image of the bulk of the film, showing the ideal $n=4$ RP structure. The unit cell is outlined in white. A simulation of the image (using the $Ca_5Mn_4O_{13}$ structure at a focus value of −150 Å and a thickness of 44 Å) is inserted inside the black frame. The indexed diffraction pattern generated as the fast Fourier transform (FFT) of the image is shown in Figure S6. Images of the $SrTiO_3$–$Ca_5Mn_4O_{13}$ interface, showing the orientation of the $Ca_5Mn_4O_{13}$ structure relative to the interface, and showing the dislocations described by the Burgers vectors b) $^1/_2\langle101\rangle_{CaMnO_3}$ and c) $\langle100\rangle_{CaMnO_3}$. The different phases are labeled, and the Burgers circuits are indicated by dashed lines.

relieved by the presence of dislocations such as the ones shown in Figure 4b and c. The Burgers circuits are indicated: the Burgers vector is $\langle100\rangle_{CaMnO_3}$ for Figure 4c and $^1/_2\langle101\rangle_{CaMnO_3}$ for Figure 4b; the latter corresponds to the insertion of a plane perpendicular to the interface as well as one parallel to the interface.

Some areas of the film contain RP layers randomly introduced along the growth direction, similar to the ones reported in films with $(SrTiO_3)_5/(SrO)_1$ superlattices.[13] An example of such an area is shown in Figure S5. On this image, one can clearly observe dark stripes perpendicular to the interface, which correspond to the contrast caused by the insertion of extra CaO layers. These defects may contribute to the reduced intensity and increased width of the low-angle (00*l*) reflections in the X-ray diffraction patterns of this and other artificial RP structures.

Thermal post-deposition annealing experiments indicate that the $n=4$ RP phase starts to decompose into the $n=\infty$ perovskite phase above 850 °C and totally disappears above 1000 °C (Figure S7). This result explains why the growth from a single bulk-composition target is unsuccessful, as the kinetic energy for surface-adatom diffusion required to rearrange the incoming atom flux from the multiphase target into the $n=4$ RP structure requires a high growth temperature (cf. the substrate temperatures of over 900 °C needed to grow the $n=$ 1 and 2 members of the RP series directly[14,24,25]). However, the annealing experiments show that the target $n=4$ RP film would not be stable under the conditions that would permit sufficient diffusion for it to form. By contrast, unit-cell-by-unit-cell modular growth with multiple targets ($CaMnO_3$ and CaO) permits each unit cell to adsorb and assemble without

the extensive reorganization required in the single-target approach.

Magnetization measurements on the films deposited are consistent with the predominantly antiferromagnetic coupling expected in these Mn^{IV} films. Chemical control of the electronic properties of the perovskite blocks by adjustment of the metals (by changing the band filling in the perovskite layers through changes to the A site cation charges) in either module or the oxygen content will be necessary to obtain metallic conductivity and ferromagnetism. The synthesis of complex oxide phases by unit-cell-by-unit-cell deposition motivated by a modular view of the target structure is a direct route to new materials in thin-film form.

Received: January 10, 2007
Revised: February 16, 2007
Published online: May 10, 2007

Keywords: electron microscopy · oxides · pulsed-laser deposition · Ruddlesden–Popper phases · thin films

[1] C. N. R. Rao, B. Raveau, *Transition Metal Oxides*, 2nd ed., Wiley, New York, **1998**.
[2] R. J. Cava, *J. Am. Ceram. Soc.* **2000**, *83*, 5.
[3] M. S. Whittingham, A. J. Jacobson, *Intercalation Chemistry*, Academic Press, New York, **1984**.
[4] A. Stein, S. W. Keller, T. E. Mallouk, *Science* **1993**, *259*, 1558.
[5] L. Fister, D. C. Johnson, *J. Am. Chem. Soc.* **1992**, *114*, 4639.
[6] D. Fischer, M. Jansen, *J. Am. Chem. Soc.* **2002**, *124*, 3488.
[7] I. Bozovic, J. N. Eckstein, *Appl. Surf. Sci.* **1997**, *114*, 189.
[8] K. Ueda, H. Tabata, T. Kawai, *Phys. Rev. B* **1999**, *60*, R12561.
[9] B. Mercey, P. A. Salvador, W. Prellier, T. D. Doan, J. Wolfman, J. F. Hamet, M. Hervieu, B. Raveau, *J. Mater. Chem.* **1999**, *9*, 233.
[10] T. Koida, M. Lippmaa, T. Fukumura, K. Itaka, Y. Matsumoto, M. Kawasaki, H. Koinuma, *Phys. Rev. B* **2002**, *66*, 144418.
[11] G. Rijnders, G. Koster, D. H. A. Blank, H. Rogalla, *Appl. Phys. Lett.* **1997**, *70*, 1888.
[12] J. H. Haeni, C. D. Theis, D. G. Schlom, W. Tian, X. Q. Pan, H. Chang, I. Takeuchi, X.-D. Xiang, *Appl. Phys. Lett.* **2001**, *78*, 3292.
[13] Y. Iwazaki, T. Suzuki, S. Sekiguchi, M. Fujimoto, *Jpn. J. Appl. Phys. Part 2* **1999**, *38*, L1443.
[14] Y. Konishi, T. Kimura, M. Izumi, M. Kawasaki, Y. Tokura, *Appl. Phys. Lett.* **1998**, *73*, 3004.
[15] L. M. Cha, P. X. Zhang, H. U. Habermeier, *Phys. B* **2003**, *327*, 163.
[16] H. Tanaka, T. Kawai, *Appl. Phys. Lett.* **2000**, *76*, 3618.
[17] Y. Takamura, R. V. Chopdekar, J. K. Grepstad, Y. Suzuki, A. F. Marshall, A. Vailionis, H. Zheng, J. F. Mitchell, *J. Appl. Phys.* **2006**, *99*, 08S902.
[18] X. L. Wang, H. Sakurai, E. Takayarria-Muromachi, *J. Appl. Phys.* **2005**, *97*, 10M519.
[19] T. Nachtrab, S. Heim, M. Mossle, R. Kleiner, O. Waldmann, R. Koch, P. Muller, T. Kimura, Y. Tokura, *J. Appl. Phys.* **2002**, *91*, 7520.
[20] P. A. Salvador, A. M. Haghiri-Gosnet, B. Mercey, M. Hervieu, B. Raveau, *Appl. Phys. Lett.* **1999**, *75*, 2638.
[21] T. Akao, Y. Azuma, M. Usuda, Y. Nishihata, J. Mizuki, N. Hamada, N. Hayashi, T. Terashima, M. Takano, *Phys. Rev. Lett.* **2003**, *91*, 156405.
[22] N. Erdman, K. R. Poeppelmeier, M. Asta, O. Warschkow, D. E. Ellis, L. D. Marks, *Nature* **2002**, *419*, 55.
[23] P. D. Battle, M. A. Green, J. Lago, J. E. Millburn, M. J. Rosseinsky, J. F. Vente, *Chem. Mater.* **1998**, *10*, 658.
[24] J. B. Philipp, J. Klein, C. Recher, T. Walther, W. Mader, M. Schmid, R. Suryanarayanan, L. Alff, R. Gross, *Phys. Rev. B* **2002**, *65*, 184411.
[25] D. G. Schlom, S. B. Knapp, S. Wozniak, L. N. Zou, J. Park, Y. Liu, M. E. Hawley, G. W. Brown, A. Dabkowski, H. A. Dabkowska, R. Uecker, P. Reiche, *Supercond. Sci. Technol.* **1997**, *10*, 891.

